IEEE Access
Multidisciplinary | Rapid Review | Open Access Journal

Received November 7, 2019, accepted November 21, 2019, date of publication November 25, 2019,
date of current version December 12, 2019.

Digital Object Identifier 10.1109/ACCESS.2019.2955713

Design of a Novel Hybrid Control Strategy for ES Grid-Connected Inverter for Smooth Microgrid Transition Operation

FENG ZHENG[1], XIANGQUN LIN[1], YANZHEN LIN[2], YACHAO ZHANG[1], AND YI ZHANG[1]
[1]School of Electrical Engineering and Automation, Fuzhou University, Fuzhou 350108, China
[2]State Grid Fuzhou Power Supply Company, Fuzhou 350000, China

Corresponding author: Feng Zheng (zf_whu@163.com)

This work was supported in part by the Natural Science Foundation of Fujian Province, China, under Grant 2019J01249.

ABSTRACT A novel hybrid control strategy for energy storage (ES) is applied in accordance to the recommendations by the IEEE Std. 1676. The strategy mainly consists of the model predictive controller (MPC), two-degree of freedom algorithm and modified droop control. In inverter control layer, MPC and two-degree of freedom algorithm are adopted to construct a generalized controller to enable ES operate in microgrid grid-connected and islanded operation modes with a single control structure, motivating the smooth transition between microgrid operating modes. And MPC and two-degree of freedom algorithm are used in the control layer's current inner loop and voltage outer loop, respectively. Comparing with the traditional double loop control from the perspective of structure, with the novel strategy the control layer's current inner loop is without pulse width modulation (PWM) and only a single proportional-integral (PI) controller is applied in its voltage outer loop, so that ES's robust performance can be enhanced. And because of the high frequency inverter's equivalent transfer function with the smaller time constant, MPC's transfer function approximated as being unitary. Therefore, when the two-degree of freedom algorithm construct the inverse model for the controlled object in control layer's voltage outer loop, from the application layer perspective, the control layer can be recognized as unity gain. Thus, the control layer's harmful disturbances associated with the operation mode transitions can be removed. In the application layer, through adding decoupling inductance and introducing microgrid's voltage and angular frequency feedforward compensations to carry out PQ and modified droop controls, the grid-connected and island control targets of ES application layer can be realized. In particular, when microgrid operation mode is switched to island, with the help of modified droop control, microgrid's voltage and frequency can be quickly restored to standard values. Through the theoretical derivation and simulation results, it can be proved that under microgrid's plan or non-plan operation mode switching, the proposed method can not only can not only implement the microgrid smooth switching, but also strengthen its transient performance.

INDEX TERMS Model predictive controllers, two-degree of freedom, smooth transition, decoupling inductance, feedforward compensation.

I. INTRODUCTION

Microgrid can reduce the negative impacts from intermittent distributed generations (DGs) on power distribution network, and maximize DGs' utilization efficiency [1]–[3]. Therefore, microgrid has been widely concerned by the academic community. By adopting the distributed generation technology, microgrid can operate in grid-connected operation and islanded operation mode [4]. ES as microgrid core equipment can not only help microgrid suppress DGs' power fluctuation and realize peak load regulation of electric power system, but also provide short-term power supply and maintain microgrid's voltage and frequency stability. In addition, comparing with other types of power supply (such as diesel engines and microturbines), ES has more flexible and convenient control effects [4]–[7]. Accordingly, ES is the key to realize the

The associate editor coordinating the review of this manuscript and approving it for publication was Guijun Li.

seamless switching of microgrid. At present, the researches about ES technology for achieving microgrid's seamless switching mainly include two aspects [8], [9].

1. How to quickly suppress the microgrid's voltage and frequency fluctuations, especially in the microgrid operation mode switching process;
2. How to eliminate or reduce the influence of harmful perturbations (contained in grid system voltage, inverter output current, etc.) on ES control system's transient performances.

To solve the first problem, the pre-synchronization technology [10], the adaptive phase-locked loop (PLL) [11], [12] and the modified droop control [13] are adopted. They are through amending the input voltage, frequency and other reference signals of ES control system to achieve microgrid seamless switching. Nevertheless, these methods ignore that the harmful disturbances which are caused by the connection line between microgrid and main network quickly being cut off or connected are injected into the ES's control system. And then they can cause microgrid's voltage distortion and grid-connected inverter overcurrent. Therefore, it is necessary to propose some related control methods to weaken or eliminate the harmful perturbation influences, so as to achieve microgrid smooth switching.

To solve the second problem, the domestic and foreign scholars also have proposed relevant methods. In [14] and [15], a feedforward signal of system voltage has been introduced into control layer to eliminate the harmful perturbation's influences on the output current of micro source. In [16]–[19], through PR and quasi-PR controllers, the voltage harmonics of the current source's control system can be filtered. In [20], based on load current feedforward control, a modified voltage controller has been adopted to improve the suppression ability of the harmful disturbances. Although the above methods can inhibit the harmful perturbations to a certain extent, eliminating the harmful perturbations completely was not possible. A generalized control algorithm for parallel inverters of DGs has been proposed to eliminate the harmful perturbations in [9]. However, because of the DGs' output power cannot be adjusted at will, under the practical circumstance, microgrid's seamless switching may be not realized. In addition, ES's robust performance in various fault conditions were not discussed in this paper. For enhancing the inverter's robust performance, a nonlinear sliding-mode voltage controller was developed to realize microgrid seamless transition in [21]. And in [20] and [22], A simple voltage controller with internal model control was developed. Similar to these approaches, the internal model controller replaced the traditional PI regulator to enhance the dynamic performance of the control system in [23]. In [24] and [25], a microgrid stabilizer using the adaptive backstepping technique is developed to guarantee robustness against unmodeled dynamics in microgrid transition. Although the inverter's robust performances were enhanced, the suppression ability improvement about the harmful disturbances was ignored. Therefore, under the microgrid

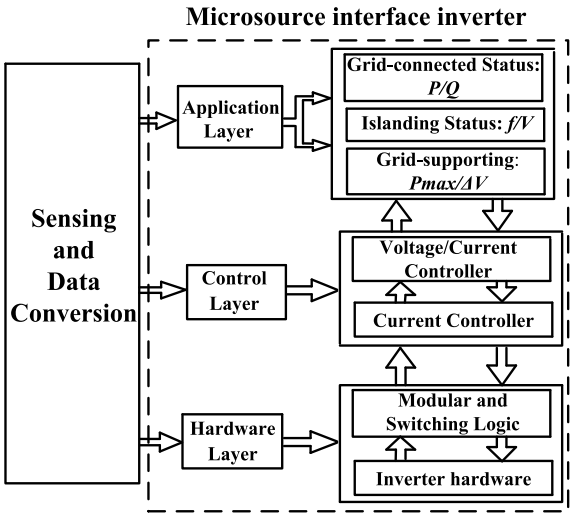

FIGURE 1. Hierarchical control structure of distributed power interface inverter.

switching process, it is necessary to design a controller with robustness, flexibility and a simple control structure to eliminate the harmful disturbance influences on ES control system and to ensure the control variable to track its input reference, rapidly and accurately.

Based on inverter's hierarchical control structure, a novel hybrid control strategy for ES is proposed to realize microgrid seamless switching. In inverter's control layer, through the model predictive controllers and two-degree of freedom algorithm, the strategy enables the control layer of ES inverter operate in all microgrid operation modes with a single control structure. And under microgrid's operation mode switching process, owing to the transfer function unitization characteristic of the control layer, the harmful perturbation influences on ES control system can be eliminated, promoting the microgrid seamless transition. In addition, the model predictive controller can also make the control layer reduce its PWM module. And there is only with single proportional-integral (PI) controller in control layer, so that the dynamic performances of control system can be significantly enhanced. In the application layer, through adding decoupling inductance and introducing microgrid voltage and angular frequency feedforward compensation to carry out PQ and modified droop controls, the smooth transition of microgrid's voltage and frequency can be realized when microgrid's operation modes switching is performed. Finally, simulation studies are also presented to validate the effectiveness of the proposed control strategy.

II. TRADITIONAL CONTROL STRATEGY OF ES GRID-CONNECTED INVERTER

According to the IEEE Std. 1676, the different functions within the control structure of ES inverter can be organized in different layers (namely, control layer, application layer and hardware layer, as shown in Fig.1 [26]). The control layer hosts the proposed multiloop controllers, which is designed to be compatible with all operating modes and to allow for

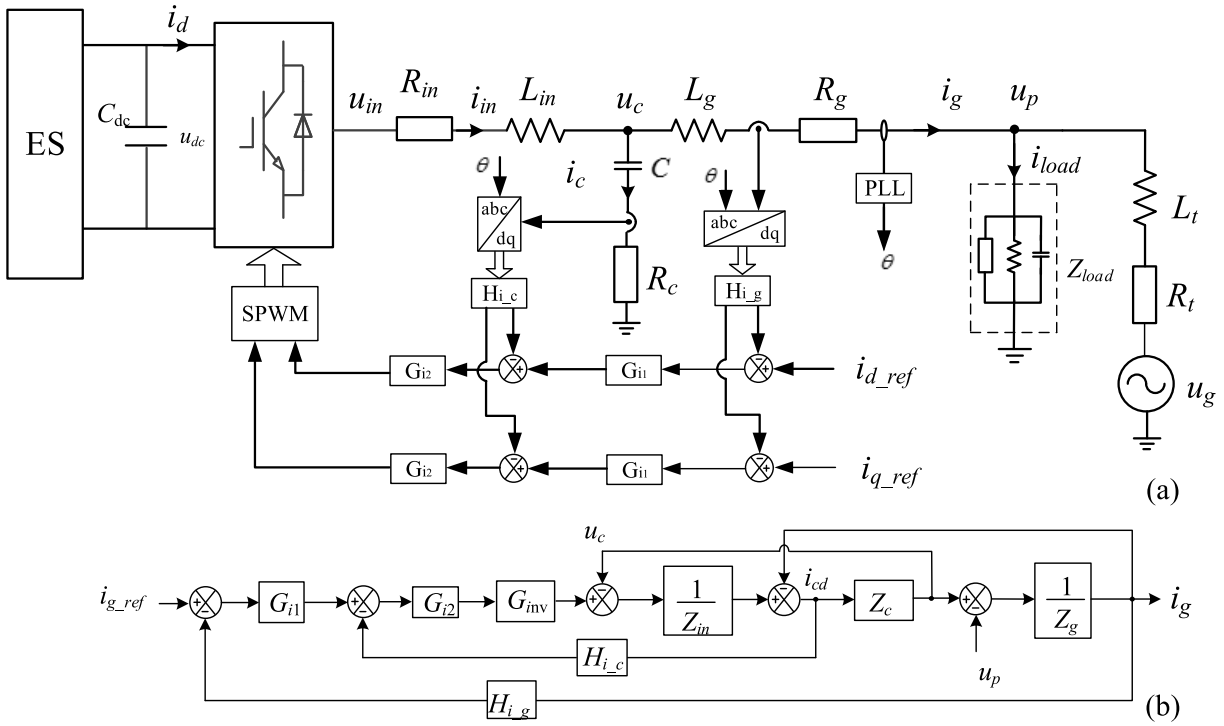

FIGURE 2. Current double closed-loop control with LCL type filter (a) structure diagram (b) control block diagram.

flexible seamless transition between them. The application control layer generates a specific reference for the control system of ES inverter according to the chosen microgrid operation mode. The functions of the hardware layer can refer to the IEEE Std. 1676.

A. TRADITIONAL CONTROL MODE OF CURRENT SOURCE AND VOLTAGE SOURCE

According to the reference signal provided by the application layer, the control modes of the control layer can be divided into current and voltage source. Referring to [27] and [28], Fig.2 and Fig.3 show the structure and control block diagrams of traditional current double closed-loop control and traditional voltage/current double closed-loop control, respectively. From Fig.2 (b), i_g can be expressed as [27]:

$$i_g = \frac{G_1(s)}{1+G_1(s)}\frac{1}{H_{i\_g}}i_{g\_ref} - \frac{G_{s2}(s)}{1+G_1(s)}u_p \tag{1}$$

Here

$$\begin{cases} G_1(s)=H_{i\_g}G_{s1}(s)G_{s2}(s) \\ G_{s1}(s)=\dfrac{G_{i1}G_{i2}G_{inv}Z_C}{Z_{in}+Z_C+H_{i\_c}G_{i2}G_{inv}} \\ G_{s2}(s)=\dfrac{Z_{in}+H_{i\_c}G_{i2}G_{inv}+Z_C}{Z_gZ_{in}+H_{i\_c}G_{i2}G_{inv}Z_g+Z_C(Z_g+Z_{in})} \\ Z_g=L_gs+R_g\ ;\ \ Z_C=\dfrac{(R_cCs+1)}{Cs}\ ;\ Z_{in}=L_{in}s+R_{in} \\ G_{inv}=\dfrac{k_{PWM}}{\tau s+1}\ ;\ G_{i1}=k_{p\_i1}+\dfrac{k_{i\_i1}}{s}\ ;\ G_{i2}=k_{p\_i2}+\dfrac{k_{i\_i2}}{s} \end{cases} \tag{2}$$

k_{PWM} and τ are the equivalent gain and switching period of interface inverter, respectively. k_{p-i1} / k_{p-i2} and k_{i-i1} / k_{i-i2} are the proportional and integral coefficients of current double-loop PI controller, respectively.

According to (1) and (2), if u_p contains lower harmonics, i_g can be influenced, especially in case of power system failure. According to Fig.3 (b), relationships between u_p and u_{p_ref} can be expressed as [28]:

$$u_p = \frac{G_2(s)}{1+G_2(s)}\frac{1}{H_{u\_p}}u_{p\_ref} - \frac{G_{T2}(s)}{1+G_2(s)}i_{DG} \tag{3}$$

Here

$$\begin{cases} G_2(s)=H_{u\_p}G_{T1}(s)G_{T2}(s) \\ G_{T1}(s)=\dfrac{G_{u1}G_{u2}G_{inv}Z_C}{Z_{in}Z_g+Z_1Z_C} \\ G_{T2}(s)=\dfrac{Z_{load}(Z_{in}Z_g+Z_1Z_C)}{Z_{in}Z_g+Z_1Z_C+(Z_{in}+Z_C)Z_{load}} \\ Z_1=H_{i\_g}G_{u2}G_{inv}+Z_g+Z_{in} \\ G_{u1}=k_{u\_i1}+\dfrac{k_{u\_i1}}{s}\ ;\ G_{u2}=k_{p\_u2}+\dfrac{k_{i\_u2}}{s} \end{cases} \tag{4}$$

k_{p-u1} / k_{p-u2} and k_{i-u1} / k_{i-u2} are the proportional and integral coefficients of voltage outer loop / current inner loop PI controller, respectively. From (3) and (4), when microgrid is in island operation mode, if Z_{load} generates harmonic generation or i_{load} /i_{DG} contains low harmonics, u_{p} will be influenced by i_g ($i_g = i_{load} + i_{DG}$), so that the island microgrid's voltage maybe not meet the power quality requirement

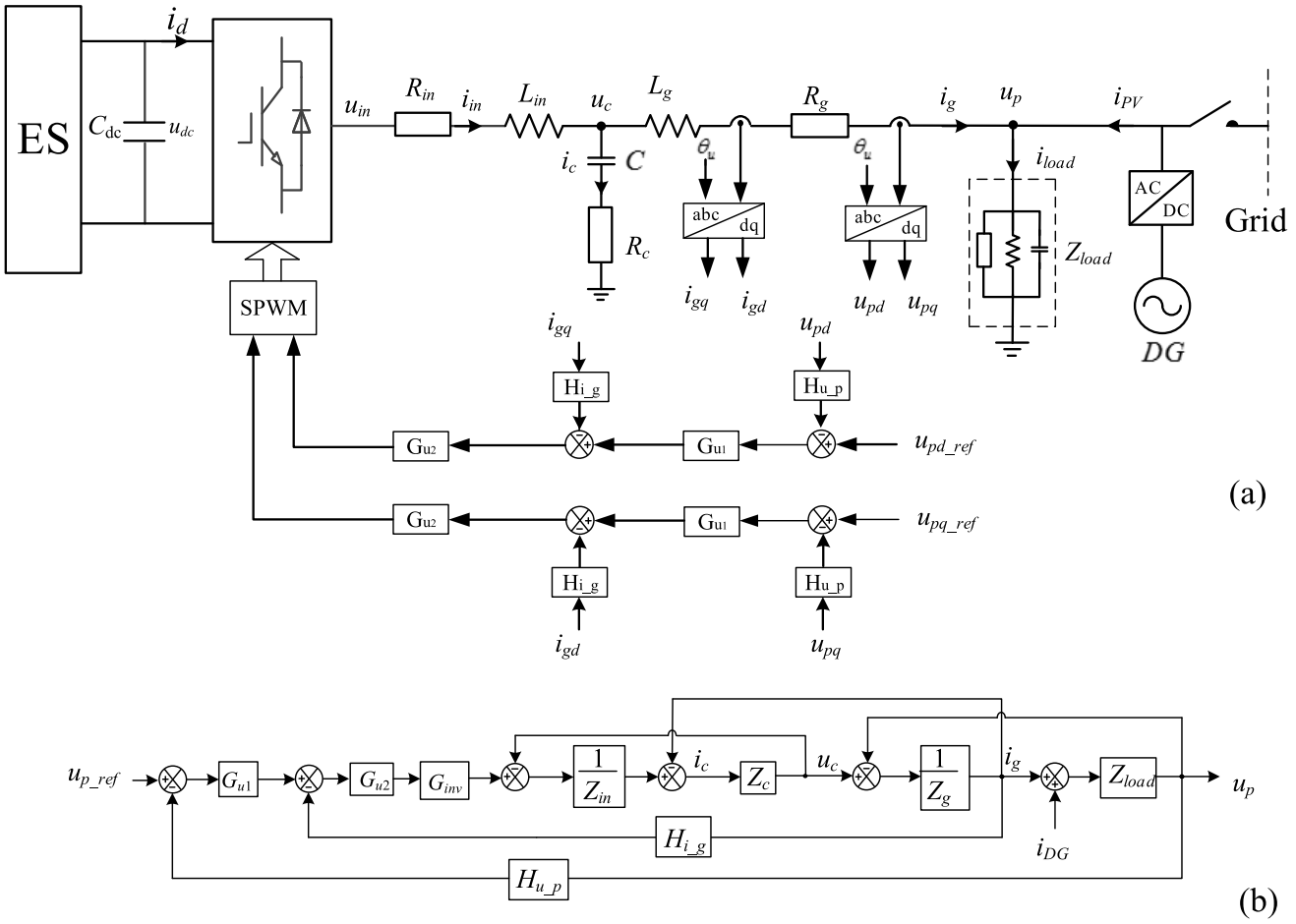

FIGURE 3. Voltage and current double closed-loop control with LCL type filter (a) structure diagram (b) control block diagram.

and the off-grid probability of voltage sensitive loads will be increased.

H_{i_g}/H_{i_c}	Grid-connected/ Capacitor current feedback coefficient
i_{gd_ref}	d axis reference current
i_{gq_ref}	q axis reference current
G_{i1}/G_{i2}	Current double-loop PI controller transfer functions
$Z_{in}/Z_c/Z_g$	*LCL* filter impedance
Z_{load}	load impedance
i_g	Inverter grid-connected current
u_p	Inverter grid-connected voltage
H_{u_g}/H_{i_g}	Grid-connected voltage/current feedback coefficient
G_{u1}	Voltage outer loop PI controller transfer functions
G_{u2}	Current inner loop PI controller transfer functions
i_{DG}	DGs output current
u_{pd_ref}	ES output d axis reference voltage
u_{pq_ref}	ES output q axis reference voltage

B. SWITCHING BETWEEN CURRENT SOURCE AND VOLTAGE SOURCE

In microgrid grid-connected mode, ES is mainly used to suppress the power fluctuation of DGs. In microgrid island mode, ES is mainly used to maintain microgrid's voltage and frequency stability. Therefore, ES grid-connected inverter has two operation modes (namely, current and voltage sources). In microgrid's operation mode switching process, ES operation mode is switched from current source to voltage source or from voltage source to current source. Comparing Fig. 3 with Fig. 2, it can be found that there are obvious structural differences between current source and voltage source. And because of harmful disturbance quantity introduced into voltage source u_p and current source i_g, the serious distortion of system bus voltage and ES overcurrent (as shown in Fig.4 [29]) can be caused and they will make microgrid's seamless switch of fail. Therefore, under ES's control strategy designing process, it is necessary to minimize the structural differences of inverter control system and eliminate the harmful disturbance influences on ES control system, so as to achieve the smooth switching of microgrid.

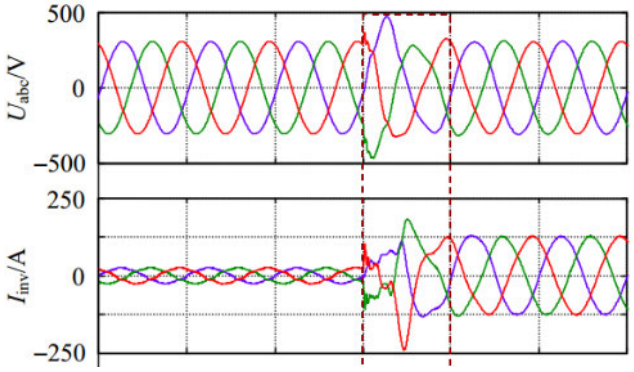

FIGURE 4. Simulation results with conventional control strategy.

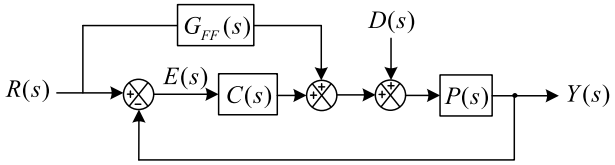

FIGURE 5. Double-freedom control system.

III. PROPOSED STRATEGY FOR ES GRID-CONNECTED INVERTER

In order to eliminate the control layer structural differences between current source and voltage source, the two degrees of freedom's control principle is adopted with *LC* type filter. Then, the unified structure of their control layer can be obtained. And for improving the dynamic performance and removing PWM of ES control system, the model predictive controllers are adopted.

A. DESIGN OF INVERTER CONTROL LAYER

Fig. 5 shows the block diagram of a two-degree of freedom control system [30]. $R(s)$, $Y(s)$, $C(s)$, $G_{FF}(s)$, $P(s)$ and $D(s)$ are the input signal, output signal, feedback controller, feedforward controller, controlled object and disturbing signal, respectively. $E(s)$ is the error between the input signal and the output signal.

According to Fig.5, the transfer functions between $R(s)$ and $Y(s)$, $R(s)$ and $E(s)$ can be expressed as follows [30]:

$$\begin{cases} Y(s)=\dfrac{C(s)P(s)+G_{FF}(s)P(s)}{1+C(s)P(s)}R(s)+\dfrac{P(s)}{1+C(s)P(s)}D(s) \\ E(s)=\dfrac{[1-P(s)G_{FF}(s)]}{1+C(s)P(s)}R(s) \end{cases} \tag{5}$$

If $G_{FF}(s)=[P(s)]^{-1}$, equation (5) is modified as:

$$\begin{cases} Y(s)=R(s)+\dfrac{P(s)}{1+C(s)P(s)}D(s) \\ E(s)=\dfrac{0}{1+C(s)P(s)}R(s) \end{cases} \tag{6}$$

Then the transfer function between $R(s)$ and $Y(s)$ has a unitary gain for all frequencies, and the optimal control for $D(s)$ can be performed through regulating $C(s)$.

In grid-connected inverter's control layer, all variables are expressed into dq coordinates. And the dynamic equations of the LC filter are expressed as [31]:

$$\begin{cases} \begin{bmatrix} u_{ind} \\ u_{inq} \end{bmatrix} = (L_{in}s+R_{in})\begin{bmatrix} i_{ind} \\ i_{inq} \end{bmatrix} - L_{in}w_0\begin{bmatrix} i_{inq} \\ -i_{ind} \end{bmatrix} + \begin{bmatrix} u_{cd} \\ u_{cq} \end{bmatrix} \\ \begin{bmatrix} u_{cd} \\ u_{cq} \end{bmatrix} = \dfrac{w_0}{s}\begin{bmatrix} u_{cq} \\ -u_{cd} \end{bmatrix} + \dfrac{(R_cCs+1)}{Cs}\begin{bmatrix} i_{ind}-i_{gd} \\ i_{inq}-i_{gq} \end{bmatrix} - \dfrac{R_cw_0}{s}\begin{bmatrix} i_{inq}-i_{gq} \\ -i_{ind}+i_{gd} \end{bmatrix} \end{cases} \tag{7}$$

L_{in} and C are the inductance and capacitance of the LC filter, respectively. R_{in} and R_c are the resistors associated with L_{in} and C, respectively. w_0 is the angular frequency. According to Fig. 5 and (7), the control layer algorithm's design diagram can be obtained as Fig. 6 shown. From Fig. 6(a), $P_1(s)0$ and $P_2(s)$ are the controlled objects. $C_1(s)$ and $C_2(s)$ are the feedback controllers of internal and external control loop, respectively. If $G_1(s) = [P_1]^{-1}$ and $G_2(s) = [P_2]^{-1}$, the results of $i^*_{in}/i_{in} = 1$, $u^*_c/u_c = 1$ can be realized. Therefore, combining Fig. 6(a) and (7), Fig. 6(b) shows the design control structure diagram of LC type control layer. From Fig. 6(b), in order to obtain $i_{in\_ref}/i_{in} = 1$, the feedforward and feedback signals can be expressed as:

$$\begin{cases} \begin{bmatrix} u_{ind\_FF} \\ u_{inq\_FF} \end{bmatrix} = G_{i\_FF}(s)D(s)\begin{bmatrix} i_{ind\_ref} \\ i_{inq\_ref} \end{bmatrix} + \begin{bmatrix} u_{cd} \\ u_{cq} \end{bmatrix} \\ \begin{bmatrix} u_{ind\_FB} \\ u_{inq\_FB} \end{bmatrix} = C_1(s)D(s)\begin{bmatrix} i_{ind\_ref} \\ i_{inq\_ref} \end{bmatrix} - C_1(s)\begin{bmatrix} i_{ind} \\ i_{inq} \end{bmatrix} \\ G_{i\_FF}(s)=R_{in};\ C_1(s)=k_{i\_p} \\ D(s)=\dfrac{L_{in}s+R_{in}+k_{i\_p}}{R_{in}+k_{i\_p}} \end{cases} \tag{8}$$

Here, i_{ind_ref}/i_{inq_ref} is the reference value of inverter output current in d/q coordinate. k_{i_p} is the feedback controller proportional gain of the current inner loop. Therefore, according to (8), Refer to the inner loop design, the feedforward and feedback output signals of the outer loop are

$$\begin{cases} \begin{bmatrix} i_{ind\_FF} \\ i_{inq\_FF} \end{bmatrix} = G_{u\_FF}(s)\begin{bmatrix} u_{cd\_ref} \\ u_{cq\_ref} \end{bmatrix} + \begin{bmatrix} i_{gd} \\ i_{gq} \end{bmatrix} \\ \begin{bmatrix} i_{ind\_FB} \\ i_{inq\_FB} \end{bmatrix} = C_2(s)\begin{bmatrix} u_{cd\_ref}-u_{cd} \\ u_{cq\_ref}-u_{cq} \end{bmatrix} \\ G_{u\_FF}(s)=\dfrac{Cs}{R_cCs+1} \\ C_2(s)=k_{u\_p}+\dfrac{k_{u\_I}}{s} \end{cases} \tag{9}$$

Here, k_{u_p} and k_{u_I} are the proportional and integral gain of the outer loop feedback controller, respectively. Accordingly, based on (8) and (9), the equation, $u_{c\_ref}/u_c = 1$, can be

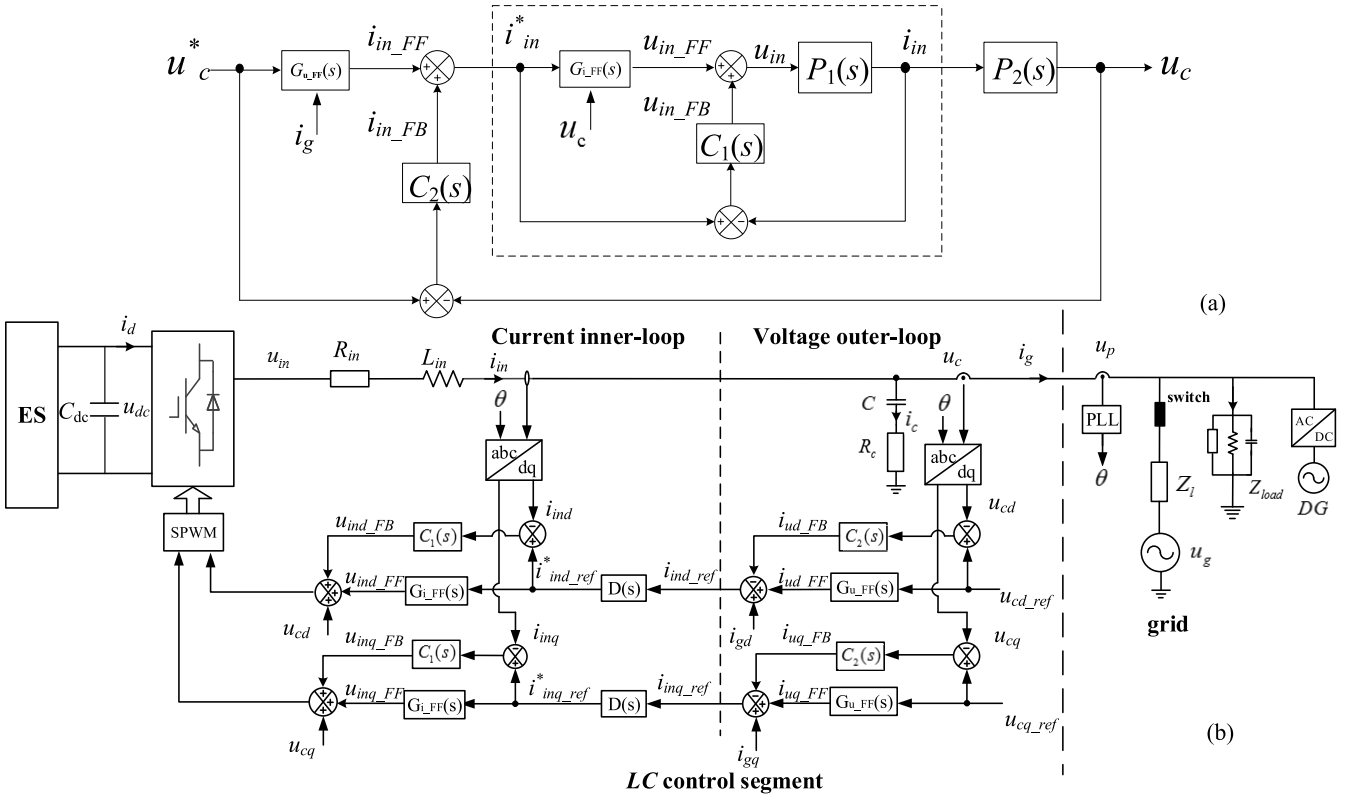

FIGURE 6. Generalized algorithm control structure diagram of LC type control layer (a) block diagram (b) control structure diagram.

realized. However, according to (7)-(9), the references signal i_{in_ref} with a differential compensation term D(s) is incorporated into the control system. The reference current $i^*_{in\_ref}$ can be expressed as:

$$\begin{bmatrix} i^*_{ind\_ref} \\ i^*_{inq\_ref} \end{bmatrix} = \frac{D(s)Cs}{R_cCs+1}\begin{bmatrix} u_{cd\_ref} \\ u_{cq\_ref} \end{bmatrix} + D(s)\begin{bmatrix} i_{gd} \\ i_{gq} \end{bmatrix} + (k_{u\_p} + \frac{k_{u\_I}}{s})D(s)\begin{bmatrix} u_{cd\_ref} - u_{cd} \\ u_{cq\_ref} - u_{cq} \end{bmatrix} \quad (10)$$

Nevertheless, D(s) has the amplification effects on the input reference signal noise. Although the effects have been discussed in [18] and most of them can be ignored, together with D(s), the noise amplification effects can't be completely ignored. In addition, owing to multiple PI controllers and D(s) connected into the control layer, the superior robustness cannot be obtained. And there are also three potential error from the established inverse model which can affect the transient performance of control layer.

In order to remove D(s) and potential error, and further enhance the robust performance of the grid-connected inverter, MPC is firstly considered for using with the two-degree of freedom algorithm in this paper. Fig. 7 shows the block diagram of MPC system [32]. u(k) and y(k) are the input signal and output signal, respectively. A and B/C are feedback controller and transfer function, respectively. 1/Z is the time delay element. From Fig.7, the relationship between u(k) and

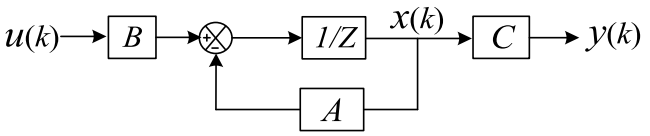

FIGURE 7. Block diagram of MPC system.

y(k) in the time of k, can be expressed as:

$$y(k+1) = CAx(k) + CBu(k) \quad (11)$$

If u(k) and y(k) are n-dimensional variable, then

$$\begin{cases} y_1(k+1) = CAx(k) + CBu_1(k) \\ \vdots \\ y_i(k+1) = CAx(k) + CBu_i(k) \qquad (i = 1, \cdots, n) \\ \vdots \\ y_n(k+1) = CAx(k) + CBu_n(k) \end{cases} \quad (12)$$

From (12), y_i(k+1) can be obtained. Hereon, y^*_i(k+1) as the reference value is introduced into MPC system. For tracing y^*_i(k + 1) accurately, f_i as value function is adopted, which can be expressed as

$$f_i = \left[y^*_i(k+1) - y_i(k+1)\right]^2 \quad (13)$$

TABLE 1. Relationship between switch states and output voltage component u_α, u_β.

STATE	g_a	g_b	g_c	u_α	u_β
S_1	0	0	0	0	0
S_2	0	0	1	$0.8165U_{dc}$	0
S_3	0	1	0	$0.4083U_{dc}$	$0.7071U_{dc}$
S_4	0	1	1	$-0.4083U_{dc}$	$0.7071U_{dc}$
S_5	1	0	0	$-0.8165U_{dc}$	$0U_{dc}$
S_6	1	0	1	$-0.4083U_{dc}$	$-0.7071U_{dc}$
S_7	1	1	0	$0.4083U_{dc}$	$0.7071U_{dc}$
S_8	1	1	1	0	0

Therefore, substituting (12) into (13), the minimum value function can be obtained

$$f_{\min} = \min(f_1, \cdots, f_n) \tag{14}$$

Then, y_i(k+1) corresponding to $f_{\min}$ will be choose to inserted into control system, so that the superior control performance can be obtained.

According to Fig.6, all variables are expressed into $\alpha\beta$ coordinates and the dynamic equations of the L_{in} filter are expressed as:

$$\begin{cases} \begin{bmatrix} u_{in\alpha} \\ u_{in\beta} \end{bmatrix} = L_{in}\dfrac{d}{dt}\begin{bmatrix} i_{L\alpha} \\ i_{L\beta} \end{bmatrix} + R_{in}L_{in}\begin{bmatrix} i_{L\alpha} \\ i_{L\beta} \end{bmatrix} + \begin{bmatrix} u_{c\alpha} \\ u_{c\beta} \end{bmatrix} \\ \begin{bmatrix} u_{in\alpha} \\ u_{in\beta} \end{bmatrix} = U_{dc}\begin{bmatrix} \sqrt{\frac{2}{3}} & -\sqrt{\frac{1}{6}} & -\sqrt{\frac{1}{6}} \\ 0 & \frac{\sqrt{2}}{2} & -\frac{\sqrt{2}}{2} \end{bmatrix}\begin{bmatrix} g_a \\ g_b \\ g_c \end{bmatrix} \end{cases} \tag{15}$$

where g_i(i = a, b, c) represent upper or lower bridge arms' switching state of three-phase grid-connected inverter. When switch off, $g_i = 1$; switch off, $g_i = 0$. Accordingly, eight switching modes of three-phase inverter can be obtained from Table 1, as well as the relationships among switching modes, DC-link voltage and the inverter output voltage. Therefore, in the time of (t_k, t_{k+1}), (15) discretization can be expressed as

$$\begin{cases} i_{L\alpha\_(k+1)} = \dfrac{T_s(u_{in\alpha\_k} - RL_f i_{L\alpha\_k} - u_{c\alpha\_k})}{L_f} + i_{L\alpha\_k} \\ i_{L\beta\_(k+1)} = \dfrac{T_s(u_{in\beta\_k} - RL_f i_{L\beta\_k} - u_{c\beta\_k})}{L_f} + i_{L\beta\_k} \end{cases} \tag{16}$$

According to Table I and (16), $u_{in\alpha}$ and $u_{in\beta}$ can be adjusted by g_a, g_b and g_c, possessing eight different output theoretical value. Then, introducing $u_{in\alpha\_k}$ and $u_{in\beta\_k}$ into (16), $i_{L\alpha-k+1}$ and $i_{L\beta-k+1}$ have eight different results. If the inverter output current is set as control target, the value function f_i can be expressed as

$$\begin{cases} f_{i\_1} = (i_{L\alpha\_ref} - i_{L\alpha1\_(k+1)})^2 + (i_{L\beta\_ref} - i_{L\beta1\_(k+1)})^2 \\ \vdots \\ \vdots \\ f_{i\_7} = (i_{L\alpha\_ref} - i_{L\alpha7\_(k+1)})^2 + (i_{L\beta\_ref} - i_{L\beta7\_(k+1)})^2 \end{cases} \tag{17}$$

Then, through substituting (16) into (17), $f_{\min}$ can be obtained. Thus, g_a, g_b and g_c (corresponding to $f_{\min}$) are implemented in the grid-connected inverter, so as to MPC can be obtained.

In order to further elucidate MPC algorithm, the flow diagram of MPC algorithm, implemented by the MATLAB, is shown in Fig.8. From Fig.8, the control loop begins sampling the voltage and current signals. Then, the algorithm estimates the grid-connected current by substituting (15) into (16), and initializes the value of the evaluated quality function f, which is a variable that will contain the value of the lower quality function evaluated by the algorithm so far. Then, the strategy, with eight possible grid-connected inverter switching state, inserts a loop where, the quality function (17) is evaluated. If, for a given switching state, f is stored as f_i, that lower value is stored as f_i, and its switching state number is stored as S_i. The loop ends when all eight switching states have been evaluated. The state that produces $f_{\min}$ is identified by the variable $S_{\min}$ and will be applied to the inverter during the next sampling interval, starting the MPC algorithm

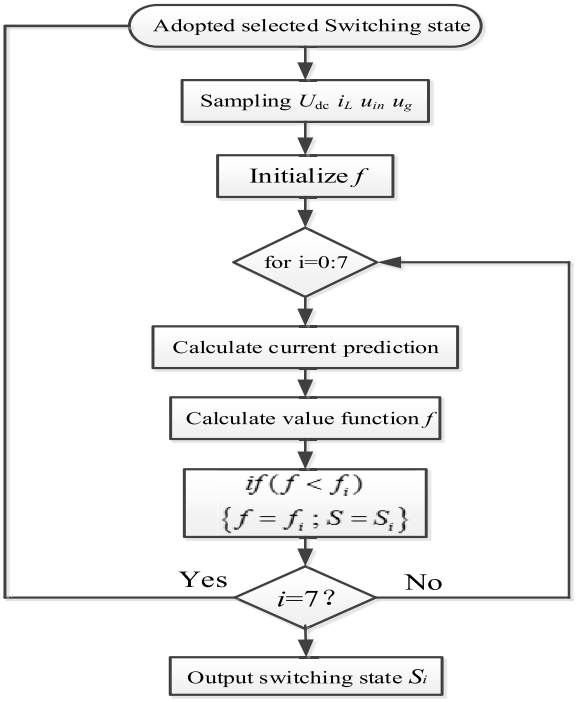

FIGURE 8. Flow diagram of the implemented MPC system.

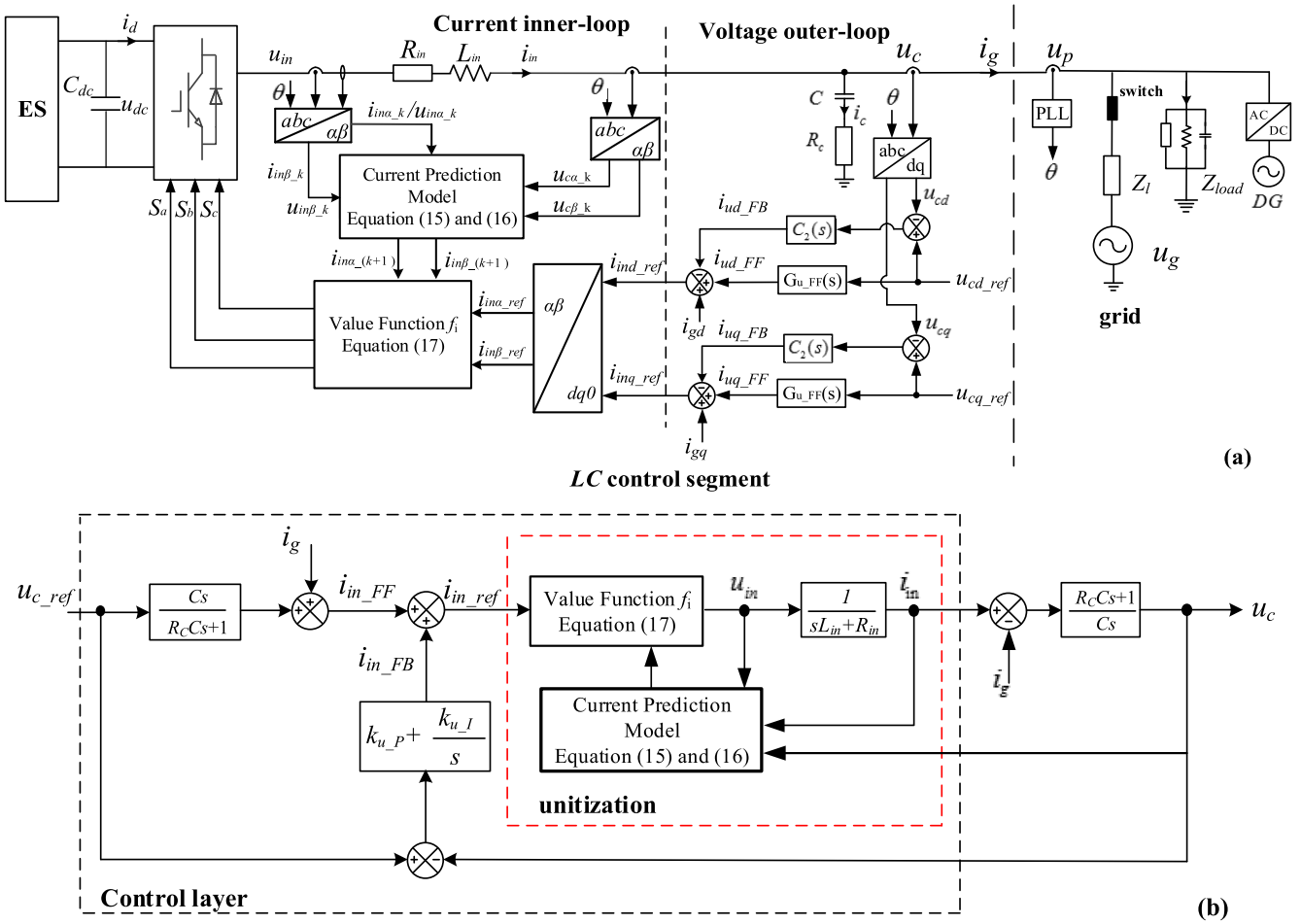

FIGURE 9. Modified algorithm of *LC* type control layer (a) control structure diagram (b) block diagram.

again. Therefore, the inverter switching state can be obtained, which can make the output quantity closest to the reference value.

Replacing the flow diagram in Fig. 8 with the current inner loop in Fig. 6, the hybrid algorithm design block diagram of *LC* type control layer can be obtained as Fig.9 shown. From Fig.9, the original PI controller of the current inner loop is changed into MPC. And the compensation term D(s) and PWM are removed. Owing to the value function f_i constructed by inverter output current and its reference quantity, and if the inverter operation frequency is set at higher value, from voltage outer loop perspective, the equivalent transfer function of MPC can be approximately equal to the equation, $k/(Ts + 1) \approx 1$ (T is the switching period and k is gain coefficient), referring to [36-38]. Therefore, from Fig.9 (b), because the transfer functions between i_{in_ref} and i_{in}, u_{c_ref} and u_c are respectively unitized, the introduced current, i_g, of the voltage outer-loop can be dynamically compensated by the grid-connected current, so that the harmful disturbance influences from i_g on the control layer can be effectively inhibited and the control system bandwidth limit can be also eliminated.

B. DESIGN OF INVERTER APPLICATION LAYER

Under different operating modes of microgrid, the unified control layer structure can't make ES unit achieve different control objectives, so that the decoupling impedance, $Z_g = R_g + jwL_g$, is introducted. Then, the various control targets (eg. P-Q, V-f and droop control) of the ES unit's application layer can be realized.

When microgrid is in the grid-connected operation mode, ES unit generally adopts P-Q control. Then, the reference voltage u_{c_ref} of control layer can be expressed as

$$\begin{bmatrix} u_{cd\_ref} \\ u_{cq\_ref} \end{bmatrix} = \begin{bmatrix} u_{pd} \\ u_{pq} \end{bmatrix} + R_g \begin{bmatrix} i_{gd\_ref} \\ i_{gq\_ref} \end{bmatrix} + k_{g\_p} \begin{bmatrix} i_{gd\_ref} - i_{gd} \\ i_{gq\_ref} - i_{gq} \end{bmatrix} \tag{18}$$

Here, R_g and L_g are the decoupling resistance and inductance, respectively. u_{pd}/u_{pq} and i_{gd_ref}/i_{gq_ref} represent the d/q axis component of the grid-connected voltage and reference current, respectively. k_{g_p} is the PI controller' scale factor. Fig.10 shows the PQ control block diagram of ES unit. From Fig.10, owing to the unitized transfer function of the control layer, the dynamic compensation is formed between the power grid voltage u_p and the introduced signal u_p.

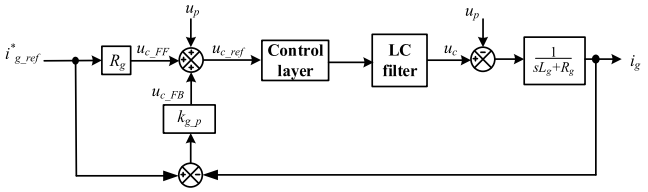

FIGURE 10. PQ control block diagram under grid-connected mode.

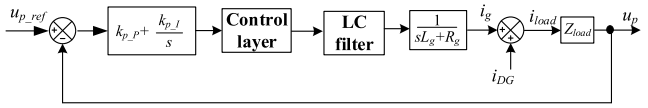

FIGURE 11. Traditional V/f control block diagram under island mode.

Therefore, the influences of harmful disturbance from the introduced signal u_p on the control system can be eliminated.

When microgrid is in the island operation mode, V-f and droop control mode are adopted to maintain microgrid's voltage and frequency stability. If ES unit adopts traditional V/f control mode (as shown in Fig. 11), the harmful disturbance from introduced signal i_{DG} can't be eliminated.

The traditional droop control's objective function is [33]:

$$\begin{cases} u = u_n + k_v(Q_{ref} - Q) \\ w = w_n + k_f(P_{ref} - P) \end{cases} \tag{19}$$

Here, u_n and w_n are microgrid rated voltage and natural angular frequency, respectively. k_v/k_f is the droop factor of P-f/Q-V control. Through using the droop control with the proposed control layer, the harmful disturbance (from i_g) influence on ES unit's control system can be eliminated. Nevertheless, when large or small disturbance occurs in the microgrid, with traditional droop control microgrid's voltage and frequency are difficult to returned to what they once to be. For removing the microgrid's voltage and frequency deviations, microgrid's angular frequency and voltage feedforward compensation are introduced to modify the traditional droop control, and it is expressed as:

$$\begin{cases} w = w_n + k_f(P_{ref} - P) + (w_n - w)(k^*_{f\_p} + k^*_{f\_I}/s) \\ u = u_n + k_v(Q_{ref} - Q) + (u_n - u_p)(k^*_{u\_p} + k^*_{u\_I}/s) \end{cases} \tag{20}$$

Here, $k^*_{f\_p}/k^*_{f\_I}$ and $k^*_{u\_p}/k^*_{u\_I}$ are the PI regulator parameters of microgrid angular frequency and voltage, respectively. Therefore, through introducing these feedforward compensation, microgrid's constant frequency and constant voltage can be obtained.

C. OPERATION MODE SWITCHING OF INVERTER

Fig. 12 shows the block diagram of the novel hybrid control algorithm. From Fig. 12, no matter the plan or unplanned operation mode of the microgrid is executed, ES only needs

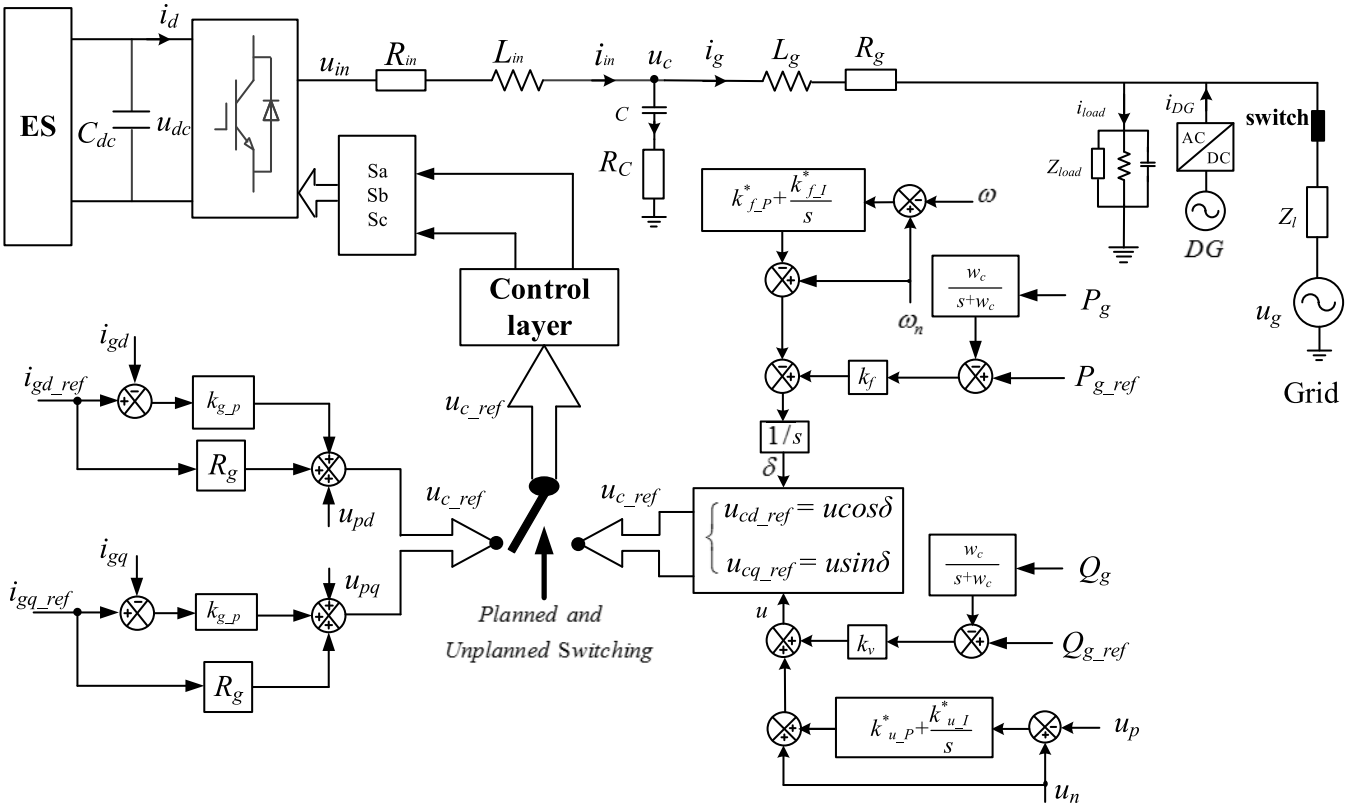

FIGURE 12. Modified algorithm control block diagram of ES inverter.

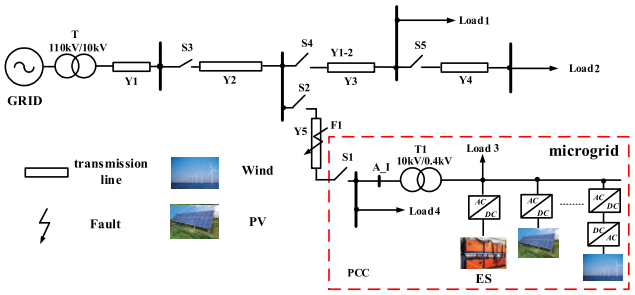

FIGURE 13. Schematic diagram of the grid-connected microgrid.

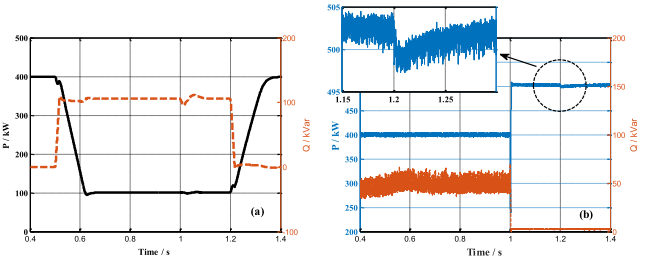

FIGURE 14. Transient curve of Micro-grid from grid-supporting to grid-forming mode (a) Output power of DGs (b) Output power of A-I point.

to switch the input signals of its application layer, so that the problems of bus voltage distortion and ES's inverter overcurrent which are caused by the structure differences of control layer can be resolved. Owing to adopting MPC and two-degree of freedom algorithm, the transfer function of

TABLE 2. Main simulation parameters of system model.

Microgrid System Simulation Parameters			
Rated Capacity T	10MVA	Load 4	500kW
Rated Capacity T1	3MVA	Wind Capacity	300kW
Transformation Ratio T	110kV/10kV	PV Capacity	100kW
Transformation Ratio T1	10kV/400V	System frequency	50Hz
Load 3	0.1MW+j0.05MVar	ES Capacity	1.4MWh
ES Control System Parameters			
L_{in}	1.5mH	R_{in}	0.15Ω
C	45μF	R_c	0.5Ω
L_g	0.5 mH	R_g	0.1Ω
k_{u_P}/k_{u_I}	1/500	$k^*_{u\_P}/k^*_{f\_P}$	1.5/3
k_f/k_v	5/2	k_{g_p}	10

control layer is united. Therefore, the input signals of the application layer can be tracked quickly and accurately, and the full dynamic compensation of the harmful disturbance can be realized. Then, the novel algorithm of ES can support microgrid to realize its smooth transition in the planned and unplanned operation modes.

IV. SIMULATION VERIFICATION

To estimate the performance of the proposed control strategy, a simulation model corresponding to Fig. 12 and 13, was created in MATLAB/SIMULINK, with parameters as shown in Table 2. According to the international operation standard

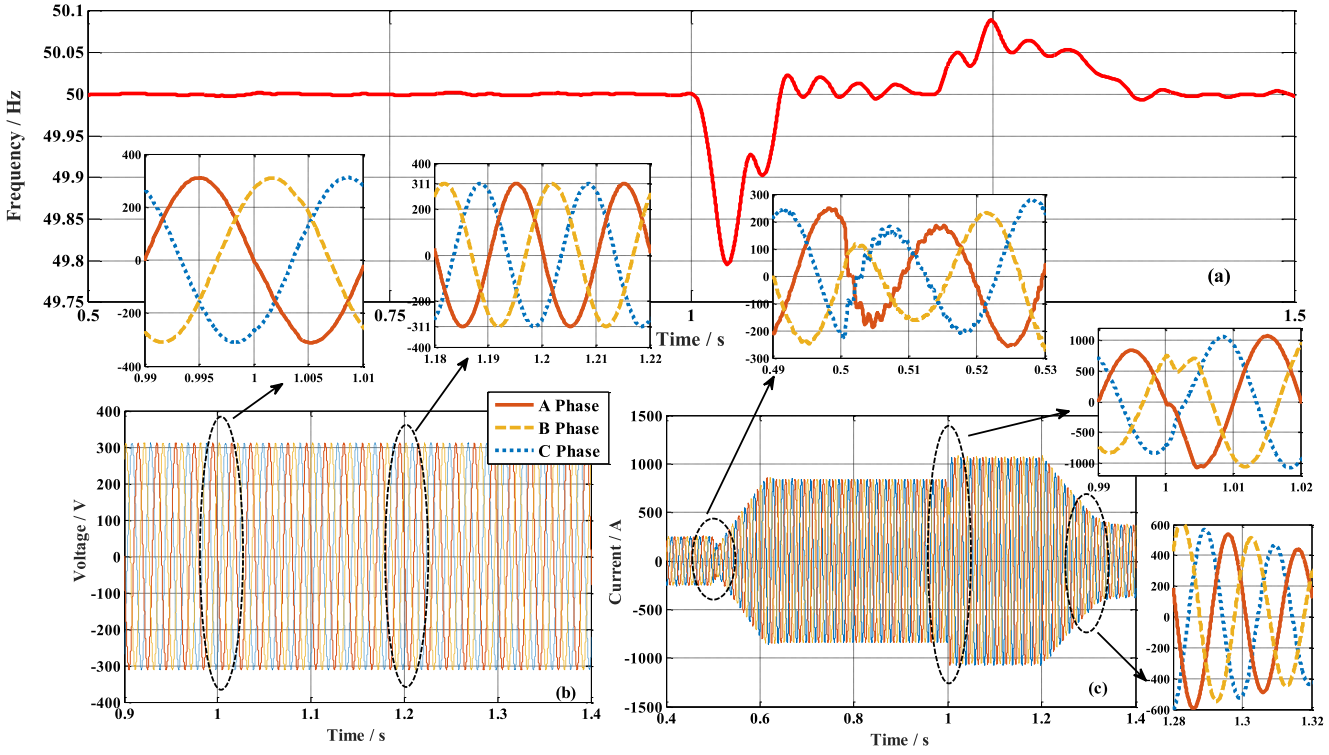

FIGURE 15. Transient curve of Micro-grid from grid-supporting to grid-forming mode. (a) Frequency Curve (b) AC-bus voltage (c) Outputs current of ES.

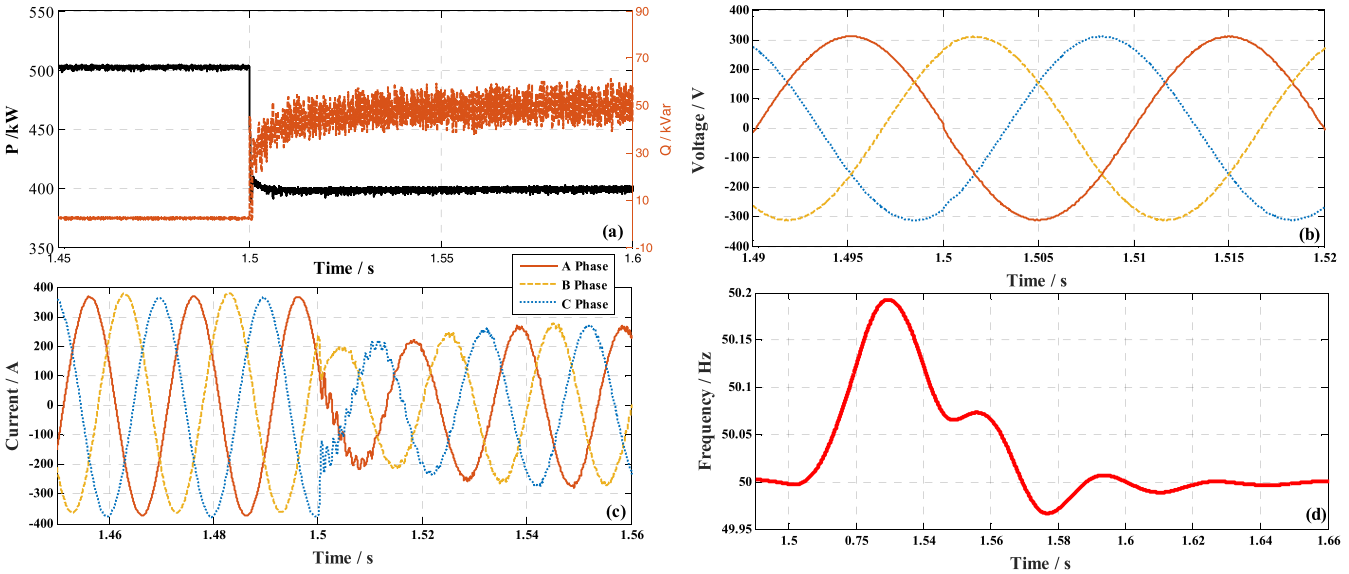

FIGURE 16. Transient curve of Micro-grid from grid-forming to grid-supporting mode. (a) Outputs power of A-I point(b) AC-bus voltage of Micro-grid (c) Output current of ES (d) Frequency.

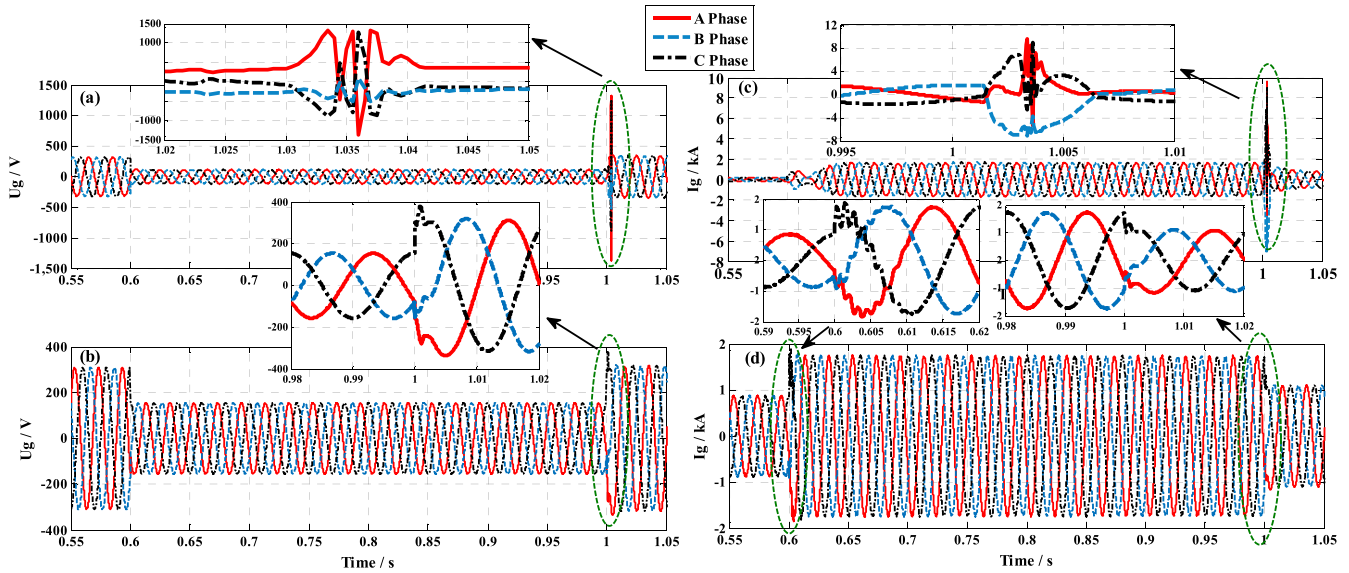

FIGURE 17. Transient curve of Microgrid from grid-supporting to grid-forming mode (a) Bus voltage with traditional control method (b) Bus voltage with the proposed method (c) Output current of A-I point with traditional method (d) Output current of A-I point with proposed method.

of microgrid, the judgment indicators of microgrid smooth switching are given in this paper.

1. In the operation mode switching process of microgrid, there are without surge current and voltage obvious distortion.
2. After operation mode switching, microgrid can quickly enter a stable operation condition. And its AC bus voltage deviation and frequency deviation are less than $7\%U_N$ (U_N presents the rated voltage) and 0.1Hz, respectively. In addition, under the operation mode switching process of microgrid, the frequency deviation, Δf, must be less than 0.5Hz.

In order to verify the effectiveness of the proposed control method, two working scenarios are adopted, namely, the planned switching and non-planned switching of microgrid operation mode. Among them, the planned switching working scenario comprises microgrid switching from grid- connection mode to isolated island mode and microgrid switching from isolated island mode to grid-connection mode. The non-planned switching working scenario is in the case of which microgrid operation mode was switched to island operation mode in the system fault condition.

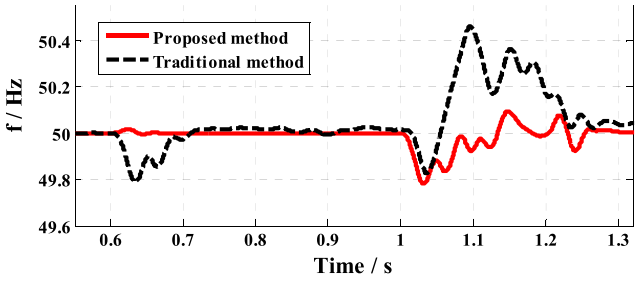

FIGURE 18. Frequency curve of Microgrid from grid-supporting to grid-forming mode.

A. MICROGRID OPERATION MODE PLANNED SWITCHING

At t = 1s, switch S_1 is disconnected (microgrid switches from grid-connection mode to isolated island mode). And it was assumed that during the operation mode switching process, the output power of microgrid's DGs and the microgrid's loads remained unchanged. Fig. 14 and Fig.15 showed the transient characteristic curve of microgrid operation mode switching process. From Fig. 14 and Fig. 15, before microgrid switches its operation mode, P/Q control mode for A-I point is adopted by ES. At t = 0.5s, although DGs' output active powers were suddenly lowered from 400kW to 100kW, as well as DGs' reactive power being increased from 0kVar to 100kVar, the output power of A-I point was still unchanged (P = 400kW; Q = 50kVar), as Fig. 14(a) and (b) shown. At t = 1s, microgrid switched from grid-connected mode to island mode. The modified droop control mode was adopted by ES to maintain the stability of microgrid's voltage and frequency. And the output power of A-I point was quickly turned into P = 500kW, Q = 0kVar, supplying power for load 4, as Fig. 14(b) shown.

From Fig. 15(a), during switching process, there was only a small microgrid's frequency fluctuation and its maximum fluctuation range didn't exceed 0.5Hz. After microgrid entering the island operation mode, its frequency deviation, Δf, was also less than 0.1Hz. Therefore, the transient performance of microgrid's frequency in the operation mode switching process can meet the given requirement. Besides, under microgrid switching process, the smooth transition of AC-bus voltage's amplitude and phase can be obtained. And its voltage deviation was less than $7\%U_N$, meeting the system voltage requirements, as Fig. 15(b) shown. From Fig. 15(c), it can be seen that when microgrid's operation mode is switched from grid-connected mode to isolated island mode, the over-current phenomenon of ES didn't occur and its smooth transition current could be also obtained. In order to further verify the anti-interference characteristic of ES, together with the modified droop control mode, it was assumed that at t = 1.2s, the output active/reactive power of DGs was suddenly changed from 100kW/100kVar to 400kW/0kVar. Then, with ES quickly responding, microgrid's power balance, voltage and frequency stabilization can be realized. And the voltage and frequency fluctuation could be also restrained into the allowable range, as Fig. 14 shown.

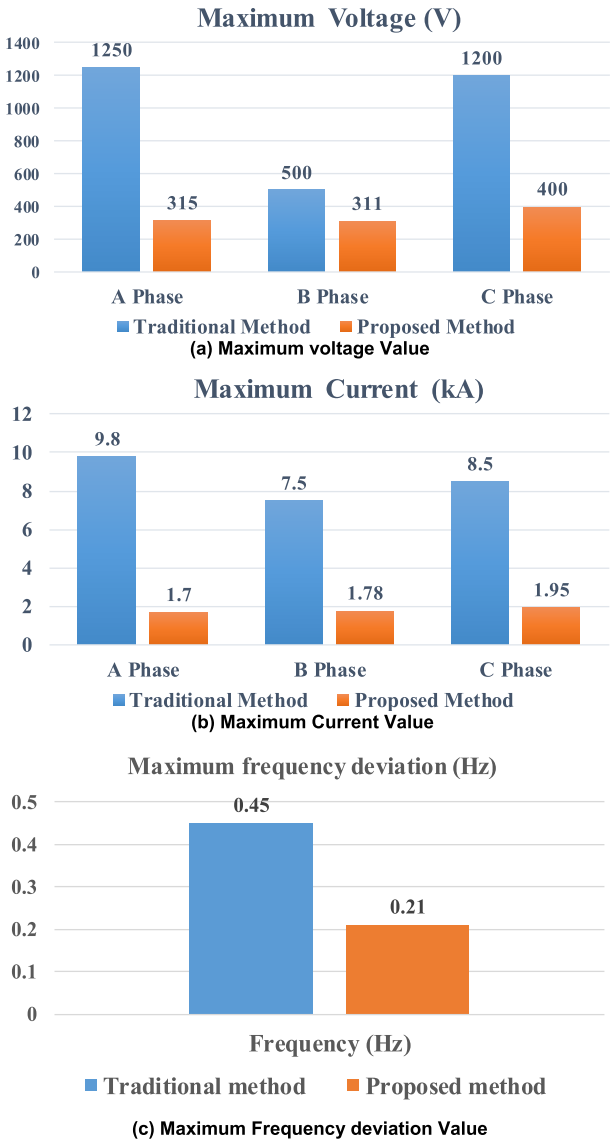

FIGURE 19. Performance comparison of microgrid voltage, current and frequency between traditional and proposed method.

At t = 1.5s, switch S_1 is closed (microgrid switches from isolated island mode to grid-connection mode). Then, the control mode of ES was transferred from the modified droop mode to PQ mode. Fig. 16 showed the microgrid's output characteristic curve, when microgrid was transferred from the isolated island mode to the grid-connection mode. The output active and reactive power of A-I point were reclassified as P = 400kW, Q = 50kVar, respectively, as Fig. 16(a) shown. According to Fig. 16 (b), the well robust and fast dynamic response features could be found. And there was without the amplitude and phase jump phenomenon of microgrid's bus voltage, so that the serious distortion of grid-connected current can be avoided, as Fig. 16 (c) shown. From Fig. 16 (d), under the grid-connection switching process of microgrid, the peak frequency deviation, Δf, was also less than 0.5 Hz. Accordingly, with the hybrid control strategy for ES, microgrid smooth switching can be achieved.

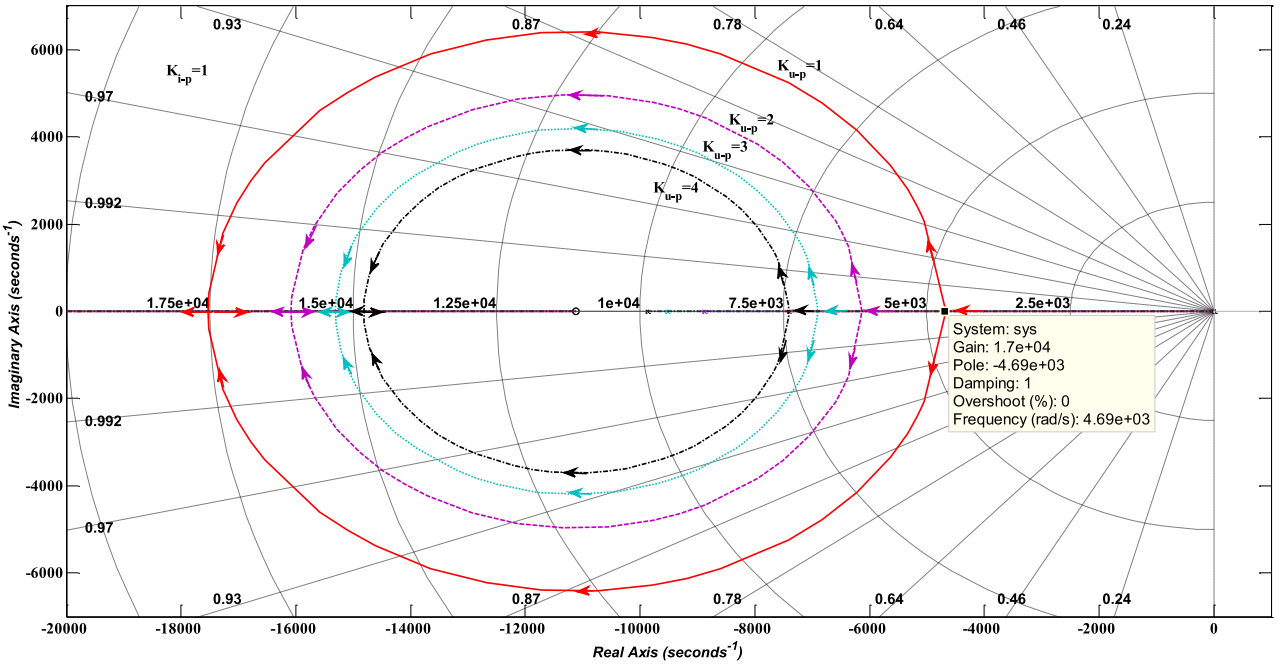

FIGURE 20. Root contours of k_{u_I}.

B. MICROGRID NON-PLAN OPERATION MODE SWITCHING

In order to further certify the transient stability characteristics of ES when a large disturbance was generated from power system, it was assumed that at t = 0.6s, three line to ground (3LG) occurred at F1 (Fig. 13). PCC voltage dropped to 50%E_N. Considering the fault detection time, the duration of 3LG was 0.4s, and then it was cleared through disconnecting S_1 at t = 1s. Therefore, the control mode of ES was switched from P/Q to V/f control mode. Fig. 17 and Fig.18 showed the transient characteristic curve of microgrid in the switching process of microgrid non-plan operation mode. According to Fig. 17(a) and (b), it can be seen that when system fault was cleared, with the proposed method microgrid operation mode was switched to island operation mode and microgrid's bus voltage distortion didn't occur. In addition, the bus voltage rapidly entered a stable operation state after the fault cleared. However, with traditional control method microgrid bus voltage was seriously distorted and had relatively longer dynamic process. From Fig. 17(c) and (d), with the proposed control method the output peak current of ES was suppressed at 1.95kA which was significantly less than the peak current 9.8kA which was with the traditional control method. Fig.18 showed the output characteristic curve of microgrid frequency in the fault process. From Fig.18, during the fault transient process, although the traditional method and the proposed method could all ensure microgrid's frequency fluctuation within the allowable range (0.5Hz), the frequency offset with the proposed method was smaller than the frequency offset with traditional method. For further demonstrating the advantages of the proposed method, Fig.19 showed the error bar to quantitative estimate how much microgrid's voltage, current and frequency fluctuations can be reduced. From Fig.19, the superior performances can be obtained with the proposed method.

V. CONCLUSION

This paper proposes a novel control method for ES to realize the smooth switching of microgrid operation mode. Based on a theoretical analysis and simulation verification, the following conclusions can be drawn:

(1) Compared with traditional methods, PWM and PI controller of the control layer's current inner loop can all be removed by MPC, so that ES's robust performance can be enhanced.

(2) From the application layer perspective, through two-degree of freedom algorithm, the control layer can be recognized as unity gain, so that the dynamic full compensation of the harmful disturbance can be realized and its influence on the control layer of ES can be removed. And under microgrid different operation modes, the control targets of ES application layer can be realized with a single control layer structure.

(3) Through introducing microgrid voltage and angular frequency feedforward compensations to carry out PQ and modified droop controls, the fluctuations of microgrid's voltage and frequency can be significantly weaken. And they are controlled in an acceptable range. Therefore, the resisting disturbance ability of island microgrid can be enhanced and it can also help

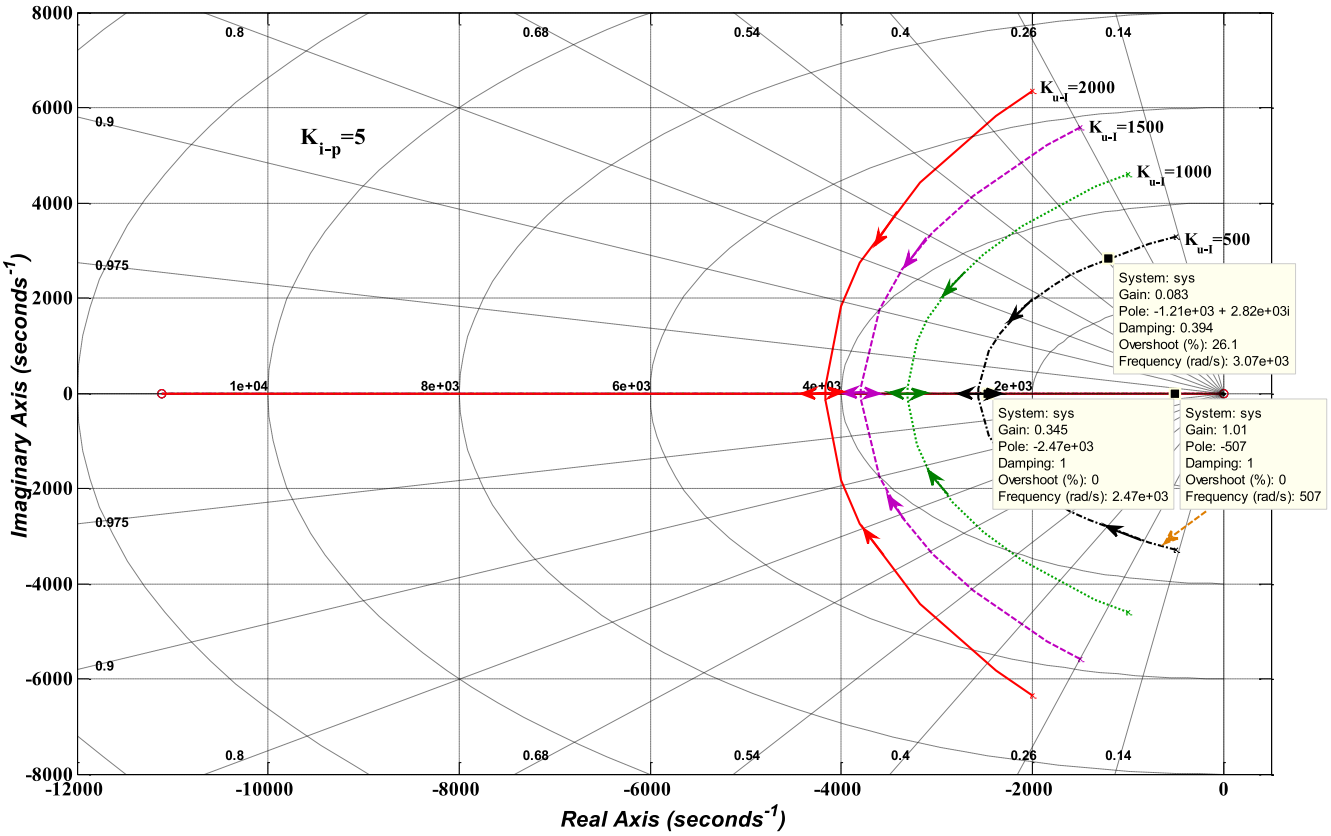

FIGURE 21. Root contours of k_{u_p}.

microgrid avoid the voltage and current distortions in its operation mode switching process. Then, the smooth switching of microgrid operation mode can be finally achieved.

APPENDIX

In this paper, the root locus method is used to discuss the controller parameters influences on the stability of control system. According to Fig. 9, the characteristic equation of the double loop is:

$$1 + \frac{(R_c C s + 1)\,(k_{u\_p} s + k_{u\_i})}{C s^2} = 0 \qquad \text{(A-1)}$$

From (A-1), there are two variables, namely, k_{u_P} and k_{u_I}. Therefore, based on (A-1), when k_{u_I} is continuously variable parameter and k_{u_P} is known parameter, the characteristic equation including k_{u_I} can be obtained as:

$$1 + \frac{k_{u\_I}(R_c C s + 1)}{C s^2 + R_c C k_{u\_P} s^2 + k_{u\_P} s} = 0 \qquad \text{(A-2)}$$

When k_{u_P} is continuously variable parameter and k_{u_I} is known parameter, the characteristic equation including k_{u_P} can be obtained as:

$$1 + \frac{k_{u\_P}(R_c C s^2 + 1)}{C s^2 + R_c C k_{u\_I} s + k_{u\_I}} = 0 \qquad \text{(A-3)}$$

Accordingly, based on (A-2) and (A-3), the characteristic equation' root locus can be obtained as Fig.20 and Fig.21 shown. From Fig.20, because all poles are in the left half plane, the system is stable. However, when k_{u_I} gets to a certain value, oscillation will occur in the system. Hence, considering system's stability and dynamic performance, k_{u_I} should be less than the value 1.7e4. According to Fig.21, its root locus is similar to Fig.20, the system is also stable. However, when the value of k_{u_P} is set too small, oscillation will also occur in the system. Therefore, according to the above analysis, the value of k_{u_P} is set as $k_{u\_P} \geq 0.35$. Then, the values of k_{u_I} and k_{u_P} are set as: $k_{u\_I} = 500$, $k_{u\_P} = 1$. Therefore, in accordance with the above method, the values of $k^*_{f\_P}$, $k^*_{u\_P}$ and k_{g_p} are set as: $k^*_{f\_P} = 3$, $k^*_{u\_P} = 1.5$ and $k_{g\_p} = 10$.

REFERENCES

[1] J. M. Guerrero, M. Chandorkar, T.-L. Lee, and P. C. Loh, "Advanced control architectures for intelligent microgrids—Part I: Decentralized and hierarchical control," *IEEE Trans. Ind. Electron.*, vol. 60, no. 4, pp. 1254–1262, Apr. 2013.

[2] M.-H. Wang, T.-B. Yang, S.-C. Tan, and S. Y. R. Hui, "Hybrid electric springs for grid-tied power control and storage reduction in AC microgrids," *IEEE Trans. Power Electron.*, vol. 34, no. 4, pp. 3214–3225, Apr. 2019.

[3] R. Lahon and C. P. Gupta, "Energy management of cooperative microgrids with high-penetration renewables," *IET Renew. Power Gener.*, vol. 12, no. 6, pp. 680–690, Apr. 2018.

[4] N. W. A. Lidula and A. D. Rajapakse, "Microgrids research: A review of experimental microgrids and test systems," *Renew. Sustain. Energy Rev.*, vol. 15, no. 1, pp. 186–202, 2011.
[5] M.-H. Wang, S. Yan, S.-C. Tan, and S. Y. Hui, "Hybrid-DC electric springs for DC voltage regulation and harmonic cancellation in DC microgrids," *IEEE Trans. Power Electron.*, vol. 33, no. 2, pp. 1167–1177, Feb. 2018.
[6] M. Ross, R. Hidalgo, C. Abbey, and G. Joós, "Energy storage system scheduling for an isolated microgrid," *IET Renew. Power Gener.*, vol. 5, no. 2, pp. 117–123, Mar. 2011.
[7] X. Zhu, X.-Q. Han, W.-P. Qin, and P. Wang, "Past, today and future development of micro-grids in China," *Renew. Sustain. Energy Rev.*, vol. 42, pp. 1453–1463, Feb. 2015.
[8] M.-H. Wang, S.-C. Tan, C.-K. Lee, and S. Y. Hui, "A configuration of storage system to reduce storage capacity in DC microgrids," *IEEE Trans. Power Electron.*, vol. 33, no. 5, pp. 3722–3733, May 2018.
[9] J. Wang, N. C. P. Chang, X. Feng, and A. Monti, "Design of a generalized control algorithm for parallel inverters for smooth microgrid transition operation," *IEEE Trans. Ind. Electron.*, vol. 62, no. 8, pp. 4900–4914, Aug. 2015.
[10] M. N. Arafat, A. Elrayyah, and Y. Sozer, "An effective smooth transition control strategy using droop-based synchronization for parallel inverters," *IEEE Trans. Ind. Appl.*, vol. 51, no. 3, pp. 2443–2454, May 2015.
[11] V. D. Bacon, S. A. O. da Silva, L. B. G. Campanhol, and B. A. Angélico, "Stability analysis and performance evaluation of a single-phase phase-locked loop algorithm using a non-autonomous adaptive filter," *IET Power Electron.*, vol. 7, pp. 2081–2092, 2014.
[12] A. Elrayyah, Y. Sozer, and M. Elbuluk, "Robust phase locked-loop algorithm for single-phase utility-interactive inverters," *IET Power Electron.*, vol. 7, no. 5, pp. 1064–1072, May 2014.
[13] H.-C. Chiang, K. K. Jen, and G.-H. You, "Improved droop control method with precise current sharing and voltage regulation," *IET Power Electron.*, vol. 9, no. 4, pp. 789–800, Mar. 2016.
[14] X. Wang, X. Ruan, S. Liu, and C. K. Tse, "Full feedforward of grid voltage for grid-connected inverter with LCL filter to suppress current distortion due to grid voltage harmonics," *IEEE Trans. Power Electron.*, vol. 25, no. 12, pp. 3119–3127, Dec. 2010.
[15] M. Xue, Y. Zhang, Y. Kang, Y. Yi, S. Li, and F. Liu, "Full feedforward of grid voltage for discrete state feedback controlled grid-connected inverter with LCL filter," *IEEE Trans. Power Electron.*, vol. 27, no. 10, pp. 4234–4247, Oct. 2012.
[16] J. Xu, S. Xie, and T. Tang, "Evaluations of current control in weak grid case for grid-connected LCL-filtered inverter," *IET Power Electron.*, vol. 6, no. 2, pp. 227–234, Feb. 2013.
[17] L. Zhou, Y. Chen, A. Luo, J. M. Guerrero, X. Zhou, Z. Chen, and W. Wu, "Robust two degrees-of-freedom single-current control strategy for LCL-type grid-connected DG system under grid-frequency fluctuation and grid-impedance variation," *IET Power Electron.*, vol. 9, no. 14, pp. 2682–2691, Nov. 2016.
[18] A. Ayad, M. Hashem, C. Hackl, and R. Kennel, "Proportional-resonant controller design for quasi-Z-source inverters with LC filters," in *Proc. IECON*, Oct. 2016, pp. 3558–3563.
[19] Y. Shi, Z. Wu, X. Dou, M. Hu, Y. Zhang, and X. Wang, "Research on phase compensation control schemes for three-phase four-wire converters," *Proc. Chin. Soc. Elect. Eng.*, vol. 37, pp. 2971–2985, May 2017.
[20] Z. Liu, J. Liu, and Y. Zhao, "A unified control strategy for three-phase inverter in distributed generation," *IEEE Trans. Power Electron.*, vol. 29, no. 3, pp. 1176–1191, Mar. 2014.
[21] Y. A.-R. I. Mohamed, H. H. Zeineldin, M. M. A. Salama, and R. Seethapathy, "Seamless formation and robust control of distributed generation microgrids via direct voltage control and optimized dynamic power sharing," *IEEE Trans. Power Electron.*, vol. 27, no. 3, pp. 1283–1294, Mar. 2012.
[22] E. N. Chaves, E. A. A. Coelho, H. T. M. Carvalho, L. C. G. Freitas, J. B. V. Júnior, and L. C. Freitas, "Design of an internal model control strategy for single-phase grid-connected PWM inverters and its performance analysis with a non-linear local load and weak grid," *ISA Trans.*, vol. 64, pp. 373–383, Sep. 2016.
[23] S. Wenxiang and Y. Yun, "A control strategy of three-phase PWM rectifier based on internal model control," *Trans. China Electrotech. Soc.*, vol. 12, pp. 94–101, Dec. 2012.
[24] S. M. Ashabani and Y. A.-R. I. Mohamed, "A flexible control strategy for grid-connected and islanded microgrids with enhanced stability using nonlinear microgrid stabilizer," *IEEE Trans. Smart Grid*, vol. 3, no. 3, pp. 1291–1301, Sep. 2012.
[25] S. Ashabani and Y. A.-R. I. Mohamed, "General interface for power management of micro-grids using nonlinear cooperative droop control," *IEEE Trans. Power Syst.*, vol. 28, no. 3, pp. 2929–2941, Aug. 2013.
[26] *IEEE Guide for Control Architecture for High Power Electronics (1 MW and Greater) Used in Electric Power Transmission and Distribution Systems*, IEEE Standard 1676-2010, Feb. 2011.
[27] X. Zhi-ying, X. Ai-Guo, and X. Shao-Jun, "Dual-loop grid current control technique for grid-connected inverter using an LCL filter," in *Proc. CSEE*, vol. 29, 2009, pp. 36–41.
[28] C. He, J. Zhao, S. Zhang, and K. Qu, "Adaptive current control strategy based on system sensitivity for grid-connected LCL-filter inverter in weak grid," in *Proc. IEEE Innov. Smart Grid Technol.-Asia (ISGT-Asia)*, Nov./Dec. 2016, pp. 418–423.
[29] C. H. E. N. Jie, C. H. E. N. Xin, F. E. N. G. Zhiyang, G. Chunying, and Y. Yangguang, "A control strategy of seamless transfer between grid-connected and islanding operation for microgrid," in *Proc. CSEE*, vol. 34, 2014, pp. 3089–3097.
[30] M. Araki and H. Taguchi, "Two-degree-of-freedom PID controllers," *Int. J. Control, Autom. Systems.*, vol. 4, no. 4, pp. 401–411, 2003.
[31] P. C. Loh and D. G. Holmes, "Analysis of multiloop control strategies for LC/CL/LCL-filtered voltage-source and current-source inverters," *IEEE Trans. Ind. Appl.*, vol. 41, no. 2, pp. 644–654, Mar. 2005.
[32] E. Z. Bighash, S. M. Sadeghzadeh, E. Ebrahimzadeh, and F. Blaabjerg, "Improving performance of LVRT capability in single-phase grid-tied PV inverters by a model-predictive controller," *Int. J. Electr. Power Energy Syst.*, vol. 98, pp. 176–188, Jun. 2018.
[33] J. Rodriguez, J. Pontt, C. A. Silva, P. Correa, P. Lezana, P. Cortes, and U. Ammann, "Predictive current control of a voltage source inverter," *IEEE Trans. Ind. Electron.*, vol. 54, no. 1, pp. 495–503, Feb. 2007.
[34] P. Cortes, G. Ortiz, J. I. Yuz, J. Rodriguez, S. Vazquez, and L. G. Franquelo, "Model predictive control of an inverter with output LC filter for UPS applications," *IEEE Trans. Ind. Electron.*, vol. 56, no. 6, pp. 1875–1883, Jun. 2009.
[35] C. Xia, T. Liu, T. Shi, and Z. Song, "A simplified finite-control-set model-predictive control for power converters," *IEEE Trans. Ind. Informat.*, vol. 10, no. 2, pp. 991–1002, May 2014.
[36] F. Zheng, C. Deng, L. Chen, S. Li, Y. Liu, and Y. Liao, "Transient performance improvement of microgrid by a resistive superconducting fault current limiter," *IEEE Trans. Appl. Supercond.*, vol. 25, no. 3, Jun. 2015, Art. no. 5602305.

FENG ZHENG was born in Wenzhou, Zhejiang, China, in 1983. He received the B.S. and M.S. degrees in electric engineering from China Three Gorges University, China, in 2006 and 2009, respectively, and the Ph.D. degree in electric engineering from Wuhan University, China, in 2017. He is currently a Lecturer with the School of Electrical Engineering and Automation, Fuzhou University. His main research interests include renewable energy fault ride through, and microgrid operation and control.

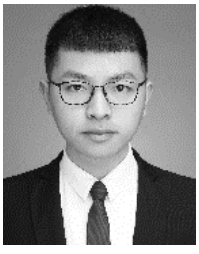

XIANGQUN LIN was born in Sanming, China, in 1996. He received the B.S. degree in electrical engineering from the College of Electrical Engineering and Automation, Fuzhou University, Fuzhou, China, in 2019, where he is currently pursuing the M.S. degree. His research interest includes suppression for resonance of grid-connected inverters in micro-grid.

YANZHEN LIN was born in Putian, Fujian, China, in 1991. She received the B.S. degree in electric engineering from the Nanjing University of Science and Technology, in 2014, and the M.S. degree in electric engineering from Wuhan University, in 2017. She is currently a Lecturer with State Grid Fuzhou Power Supply Company. Her main research interests include renewable energy, energy storage, and microgrid.

YACHAO ZHANG received the B.S. and M.S. degrees in water conservancy and hydropower engineering from the Huazhong University of Science and Technology, Wuhan, China, in 2007 and 2010, respectively, and the Ph.D. degree in electrical engineering from Wuhan University, Wuhan, in 2017. He is currently a Lecturer with the School of Electrical Engineering and Automation, Fuzhou University. His main research interests include power system optimization dispatch with renewable energy, and wind power forecast.

YI ZHANG was born in Fujian, China. He received the B.S. and Ph.D. degrees from Sichuan University, Sichuan, China, in 2007 and 2012, respectively. From 2012 to 2014, he was a Postdoctoral Fellow with State Grid Fujian Electric Power Company and Zhejiang University. From 2015 to 2017, he was a Senior Engineer with the State Grid Power Quality Analysis Laboratory, State Grid Fujian Electric Power Research Institute. He is currently an Associate Professor with Fuzhou University, Fujian. His research interests include the active distribution systems, power quality, and distributed energy resource operating and control.